NASA Technical Memorandum 104824

Flight Test Results from Real-Time Relative Global Positioning System Flight Experiment on STS-69

Young W. Park
Jack P. Brazzel, Jr.
J. Russell Carpenter
Heather D. Hinkel
James H. Newman

November 1996

NASA Technical Memorandum 104824

Flight Test Results from Real-Time Relative Global Positioning System Flight Experiment on STS-69

Young W. Park
Jack P. Brazzell, Jr.
McDonnell Douglas
Houston, Texas

J. Russell Carpenter
Heather D. Hinkel
James H. Newman
Lyndon B. Johnson Space Center
Houston, Texas

November 1996

This publication is available from the NASA Center for Aerospace Information, 800 Elkridge Landing Road, Linthicum Heights, MD 21090-2934, (301) 621-0390

Contents

Figures

Acronyms

ATV	automated transfer vehicle
BET	best estimated trajectory
C/A	coarse/acquisition
cg	center of gravity
DVM	dual-vehicle mode
ESA	European Space Agency
FOM	figure of merit
GPC	general-purpose computer
GPS	global positioning system
GUI	graphical user interface
ISS	International Space Station
JPL	Jet Propulsion Laboratory
LVLH	local vertical/local horizontal
MCC	Mission Control Center
RGPS	relative global positioning system
RNAV	rendezvous navigation
RPOP	rendezvous and proximity operations program
SA	selective availability
SMA	semimajor axis
STS	Space Transportation System (the Space Shuttle)
SVM	single-vehicle mode
TDRSS	tracking and data relay satellite system
TRAD	tools for rendezvous and docking
UT/CSR	University of Texas Center of Space Research
WSF	Wake Shield Facility

Abstract

A real-time relative global positioning system (GPS) Kalman filter has been developed in support of automated rendezvous with the International Space Station (ISS). The filter is integrated with existing Space Shuttle rendezvous software running on a 486 laptop computer under Windows®. In this work we present real-time and postflight results achieved with the filter on Space Shuttle mission STS-69. This experiment used GPS data from an Osborne/Jet Propulsion Laboratory (JPL) TurboRogue receiver carried on the Wake Shield Facility (WSF) free-flyer and a Rockwell Collins 3M receiver carried on the Orbiter. Real-time filter results, processed onboard the Shuttle and replayed in near-real-time on the ground, are based on single-vehicle mode operation and on 5 to 20 minute snapshots of telemetry provided by WSF for dual-vehicle mode operation. Postflight results were achieved by running the filter in a real-time mode using data recorded during the mission.

Orbiter and WSF state vectors calculated using our filter compare favorably with precise reference orbits determined by the University of Texas Center for Space Research. The reference orbits were generated by double-differencing GPS data from both vehicles along with data from GPS ground stations. The lessons learned from this experiment will be used in conjunction with future experiments to mitigate the technology risk posed by automated rendezvous and docking to the ISS.

Introduction

We have developed a real-time relative global positioning system (RGPS) extended Kalman filter in support of automated rendezvous with the International Space Station (ISS) (ref. 1), based in part on earlier work by Montez and Zyla (ref. 2). The filter design exploits common satellite tracking by both chaser and target vehicle receivers, and optimizes its performance during periods of asynchronous tracking. The filter is integrated with existing Space Shuttle rendezvous support software running on a 486 laptop computer under Windows®. The filter is designed to support a wide variety of global positioning system (GPS) receivers under adverse selective availability (SA) conditions. Handover at close range to a proximity operations sensor precludes the need for sub-decameter solution accuracy. Therefore, the filter processes coarse/acquisition (C/A) code pseudo-range measurements only.

To mitigate the technology risk posed by automated rendezvous and docking to the ISS, an RGPS experiment will be performed on STS-80. STS-69 provided an opportunity for incremental software development, early software validation, and valuable experience processing real-time RGPS data prior to this important milestone. We will apply the lessons learned from the experiment on STS-69 to ensure successful results on STS-80.

In this work, we will present real-time and postflight results achieved with the filter on Space Shuttle mission STS-69. We will first present a summary of the experiment mission plan and objectives. Then we will include crew member comments, flight experiment setup, and challenges encountered. Next, we will discuss the integration of the filter into the rendezvous and proximity operations program (RPOP). Following this discussion will be a description of the filter design itself. We will then present results for single- and dual-vehicle filter operation, both from real-time processing and from postflight analysis, by running the filter in a real-time mode using data recorded during the mission. We will present a comparison of the Orbiter and Wake Shield Facility (WSF) state vectors calculated using our filter to those from precise reference orbits determined by the University of Texas Center of Space Research (UT/CSR) (ref. 3). Finally, we will conclude with a summary of results and lessons learned.

Mission Summary and Objectives

The experiment involved a GPS receiver on both the Orbiter and the WSF free-flyer. Throughout this paper we will use Orbiter and "chaser" interchangeably and WSF and "target" interchangeably. Orbiter GPS data

were available onboard continuously throughout the mission, while the WSF GPS data were only available intermittently. The plans for real-time relative GPS data collection during WSF free-flight consisted of several short snapshots of WSF GPS data followed by continuous data during the rendezvous. The snapshots were intended to test the space-to-space communications link and to make a quick assessment of the WSF GPS data. The continuous data period was intended to prove the operation and accuracy of the real-time RGPS filter in a rendezvous environment. Unfortunately, continuous WSF GPS data transmission did not occur because of a failure in the power supply to the receiver. Fortunately, 19 hours of WSF GPS data were recorded onboard the free-flyer prior to the power supply failure. These problems restricted the filter operation to single-vehicle mode (SVM) during most of the mission. The snapshots provided limited operation in dual-vehicle mode (DVM), however. The experiment objects, specified by Hinkel et al. (ref. 1), are listed below:

1. Collect flight experiment GPS data that will support the European Space Agency (ESA) in validating the automated transfer vehicle (ATV) ground verification facilities (specifically GPS models used in the facility).

2. Determine the accuracy of GPS relative navigation, including usable ranges.

3. Learn the effect of common versus non-common satellite tracking between two different receivers.

4. Gain experience in passing GPS data through a space-to-space communications link for real-time navigation.

Unfortunately, all objectives were not met during the mission. Most of the objectives were achieved, however, by processing both WSF and Orbiter GPS data post-mission. Objective 1 was accomplished by recording significant amounts of GPS data onboard each vehicle. Objective 2 was partially achieved by comparing the RGPS filter results to a best estimated trajectory (BET). The anticipated accuracy was not achieved owing to unexpected marginal GPS receiver performance. Objective 3 was met by quantifying the negative effect of non-common satellite tracking between two different receivers using the flight data. The first part of Objective 4 was met by successfully transmitting WSF GPS data through the space-to-space communications link during the snapshots. To fulfill Objective 4 completely, successful onboard real-time relative navigation was required. This did not occur, however, and postflight analysis operating the filter with recorded data allowed the rest of Objective 4 to be partially fulfilled. Although all objectives were not completely achieved, we learned many lessons and gained valuable experience in preparation for STS-80.

Crew Member Comments

Mission Specialist Jim Newman operated the experiment inside the Orbiter cockpit throughout the STS-69 mission. Following is a commentary on the experiment from Dr. Newman's perspective:

"STS-51 was the first time a GPS unit was flown on the Shuttle, successfully determining Orbiter state vectors (ref. 4). STS-51 also included another GPS unit on a deployed satellite, ORFEUS-SPAS. Although the GPS data were displayed on an onboard laptop, no attempt was made to do true relative GPS state vector determination at that time. But it was clear that GPS had tremendous potential. Although the primary emphasis on STS-69 is application to automated rendezvous, Shuttle crews expect to benefit as well. The addition of GPS and relative GPS sensor information to the suite of available rendezvous and proximity operations tools may help reduce propellant budget and increase our margin for mission success. Operating this experiment on orbit was time-consuming and somewhat frustrating because of a number of unforeseen anomalies. However, it is still felt that the efforts were worthwhile for this step in the development of GPS as a standard method for accurate orbit and relative position determination."

Flight Experiment Setup

To fulfill onboard real-time data processing objectives, three Orbiter laptop computers were linked to route the data for processing, as shown in Figure 1. RPOP with the integrated RGPS filter (RPOP/RGPS)

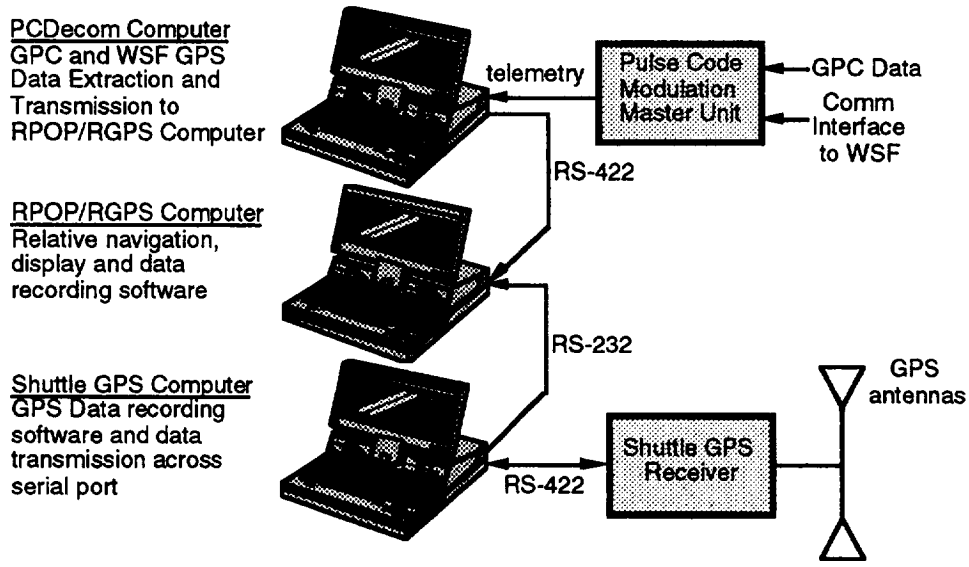

Figure 1: Onboard laptop computer setup

resided on one laptop computer. It received WSF GPS measurements and solutions, Orbiter GPS measurements and solutions, and navigation data from the Orbiter general-purpose computer (GPC). A second laptop containing a software package called PCDecom stripped the real-time GPC and WSF GPS data from the telemetry, decommutated the original data, and transmitted formatted data packets to RPOP/RGPS via RS-422 serial connection. The third laptop, containing the Orbiter GPS receiver command, control, and display software, transmitted the Orbiter GPS data to RPOP/RGPS via RS-232 serial connection.

The experiment used GPS data from an eight-channel Osborne/Jet Propulsion Laboratory (JPL) TurboRogue receiver carried by the WSF free-flyer, and a Rockwell Collins 3M receiver carried on the Orbiter, as described by Schutz et al. (ref. 5). A single GPS antenna was mounted on the WSF free-flyer. Two GPS antennas were mounted on the Orbiter. One of the GPS antennas is located on top of the Orbiter and the other on the bottom of the Orbiter, as seen in Figure 2. The 3M receiver takes inputs from both antennas and selects a set of four GPS satellites based on the selection algorithm. The receiver does not know which antenna is tracking which GPS satellites, so the antenna-to-center of gravity (cg) offset is not precisely known.

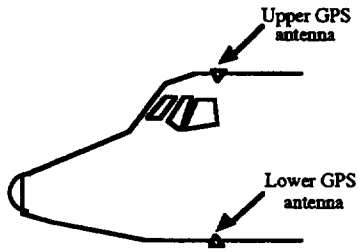

Figure 2: Orbiter GPS antenna locations

Integration of RPOP and RGPS

To accomplish Objective 4 of the flight experiment – performing relative GPS data filtering in real time onboard the Space Shuttle – we integrated the RGPS filter into an already existing Shuttle flight-certified software program called RPOP. We chose to integrate RGPS into RPOP because:

- RPOP was flight certified and used as a standard tool on every Shuttle rendezvous and deploy mission
- the STS-69 crew was very familiar with RPOP and had used it on previous rendezvous flights
- RPOP had the framework for a GPS data interface
- RPOP was originally designed to allow easy integration of new sensors, such as GPS
- RPOP provides a long-term platform for GPS data processing onboard the Shuttle

RPOP is a Windows® application that runs on a laptop computer in the Shuttle's cockpit during rendezvous, docking, and deploy missions. RPOP provides useful information, not available on standard Orbiter displays, to assist the Shuttle crew during rendezvous and proximity operations with other spacecraft. RPOP displays navigation and guidance information based on Orbiter data and sensor measurements. In addition, RPOP is the heart of the Shuttle tools for rendezvous and docking (TRAD) system used for Shuttle-to-Mir and, eventually, for Shuttle-to-ISS rendezvous and docking missions.

RPOP provides a dynamic picture of the Shuttle's current position relative to the rendezvous target, and predicts its future trajectory. RPOP processes data from various sensors including radar, payload bay laser, handheld laser, and closed-circuit television cameras, as well as navigation data from the onboard GPCs. Figure 3 shows a snapshot of the RPOP relative motion display using recorded data taken from STS-69. Figure 4 shows the same trajectory, zoomed in.

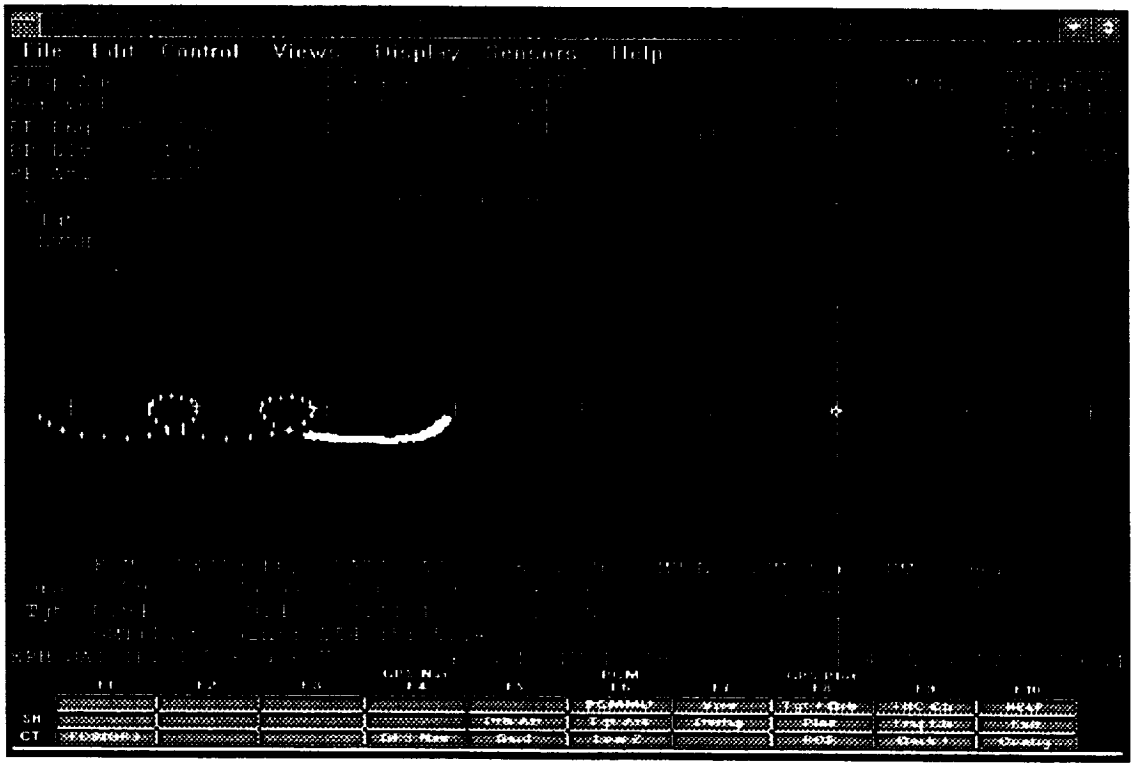

Figure 3: RPOP relative motion display using recorded data

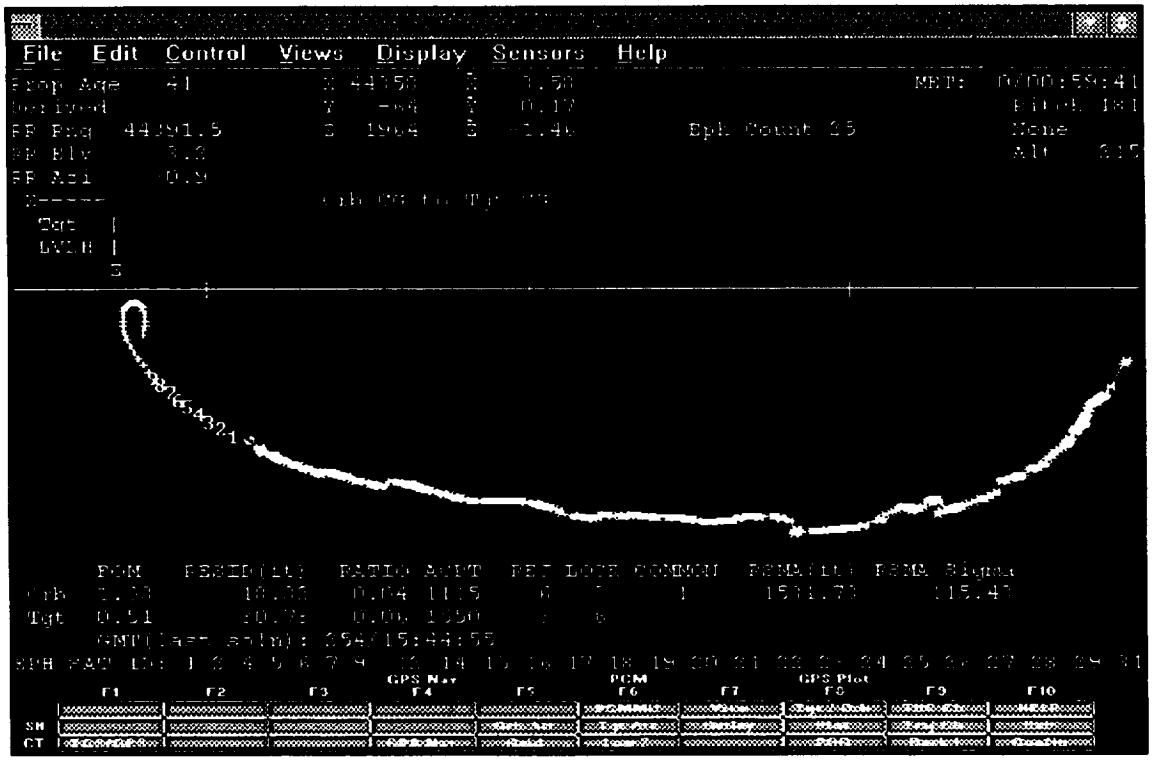

Figure 4: RPOP zoomed-in relative motion display using recorded data

Several modifications were made to RPOP to accommodate the RGPS filter including:

- external data interfaces to allow RPOP to receive GPS data via serial connection
- logic to schedule the RGPS filter execution and (re)initialization
- link between RPOP and RGPS using a Dynamic Link Library
- navigation modules to compute relative states based on deterministic GPS solutions
- additions to the graphical user interface (GUI) to provide the user with GPS and RGPS data display configuration options

For this experiment, the Orbiter GPS data were available at 0.5 Hz; the WSF GPS data were only available at 0.2 Hz. As a result, the filter was designed to execute with new measurement data at 0.2 Hz. The Orbiter GPS data are stored in a buffer to allow time synchronization with the WSF GPS measurements. Initially, if WSF GPS measurements are not available, the filter initializes in SVM. However, as soon as WSF GPS measurements become available, the filter automatically reinitializes and operates in DVM. The filter also reinitializes automatically if the figure of merit (FOM) for the chaser or target exceeds 50.0.

A new GUI was added to RPOP to accommodate the GPS data. It provides control initialization of the RGPS filter and display of filter performance parameters (shown at the bottom of the RPOP display in Figure 4). The GUI is also designed to allow the crew to compare any combination of chaser and target state vectors from the Shuttle onboard rendezvous navigation (RNAV), the GPS, or the RGPS filter. Figure 5 shows the RPOP dialog box with all possible state vector display options. This design allows the crew not only to see real-time relative motion, but also to view differences between two sources of chaser or target state vectors.

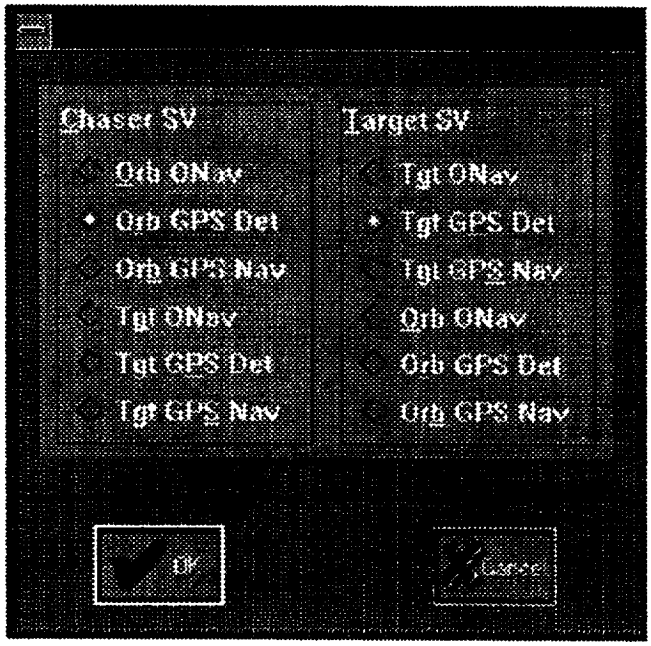

Figure 5: RPOP state vector configuration dialog box

Relative GPS Kalman Filter Design

To accomplish GPS orbit determination in periods when the space-to-space communications link from the WSF is unavailable, the filter is designed with two modes of operation: SVM and DVM. Since similar models are used in both, we will first describe the SVM design, then point out the additions for the DVM design. The discussion below is a summary of the models, assumptions, and approximations in the filter. The filter architecture is shown in Figure 6.

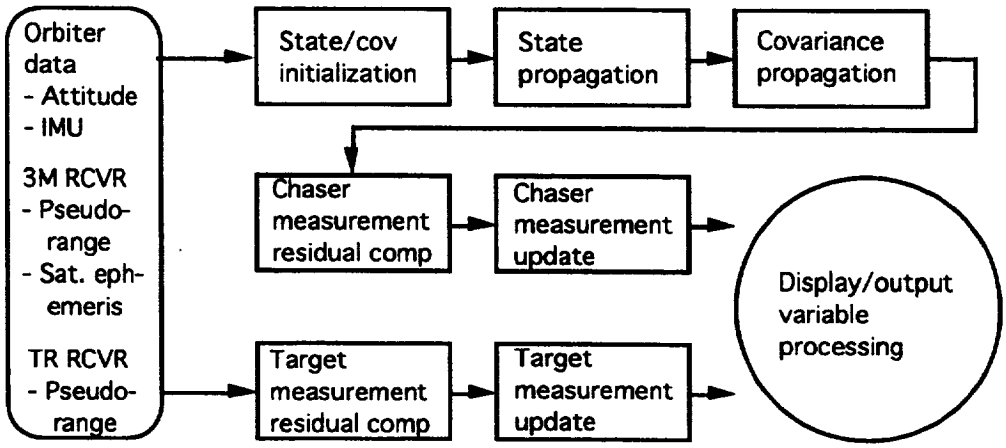

Figure 6: RGPS filter architecture

Single-Vehicle Mode

The RGPS filter operates in Earth-centered, Earth-fixed coordinates. It assumes the following model for the time evolution of the Orbiter position and velocity.

$$\begin{gathered}\ddot{\mathbf{r}}_c(t) = \dot{\mathbf{v}}_c(t) = \mathbf{f}_{nm}(\mathbf{r}_c(t)) + \omega_E \times \omega_E \times \mathbf{r}_c(t) - 2\omega_E \times \mathbf{v}_c(t) + \mathbf{a}_s(t) + \delta\mathbf{a}_u(t) + \mathbf{w}_d(t) \\ \mathrm{E}[\mathbf{w}_d(t)] = 0, \quad \mathrm{E}[\mathbf{w}_d(t)\mathbf{w}_d^{\mathrm{T}}(\tau)] = \sigma_{wd}^2 \delta(t-\tau)\mathbf{I}\end{gathered} \tag{1}$$

In (1), t represents time, the variable over which the differentiation indicated by the overdots occurs, $\mathbf{r}_c$ is the chaser vehicle (Orbiter) position, $\mathbf{v}_c$ is the chaser velocity relative to the Earth-fixed rotation frame, ω_E is the Earth's angular velocity vector, and the symbol x represents the cross-product operator. Also, $\mathbf{f}_{nm}$ is a truncation of the GEM-10 gravitational force model (ref. 6) to degree n and order m; although we typically operate the filter with $n = m = 4$, the filter has coefficients up to degree and order 30. The acceleration sensed by accelerometers onboard the Orbiter during powered flight is $\mathbf{a}_s$. The remaining two terms are random disturbances. The first of these, $\delta\mathbf{a}_u$, we refer to as "unmodeled acceleration." We tune this to accommodate other time-correlated forces acting on the vehicle such as drag, continuous or relatively long-duration vehicle venting, and gravity model errors. The unmodeled acceleration is assumed to evolve as a vector of uncorrelated first-order Gauss-Markov process (ref. 7, pp. 81-82), equally distributed among its three coordinates. We include the second term, $\mathbf{w}_d$, termed direct process noise, to model timewise uncorrelated forces, including short-duration vents and uncoupled attitude maintenance maneuvers, among others. In specifying the statistics of $\mathbf{w}_d$, we denote the expectation operator by the letter E, the transpose operation by the superscript T, the identity matrix by I, and the Dirac delta function by $\delta(t-\tau)$. The variable σ_{wd}^2 is the noise variance.

The filter processes a discrete sequence of pseudorange measurements for the chaser, from up to four GPS satellite vehicles at a time, that we assume are modeled as follows:

$$\begin{gathered}\rho_{SVi}(t_j) = \left\|\mathbf{r}_c(t_j) - \mathbf{r}_{SVi}(t_j + \delta t_T)\right\| + c(t_j) + I_{SVi}(t_j) + b_{SVi}(t_j) + v_j, \\ \mathrm{E}[v_j] = 0, \quad \mathrm{E}[v_j v_k] = \sigma_v^2 \delta_{jk}, \quad j = 1,2,\mathrm{K}\end{gathered} \tag{2}$$

In (2), t_j is the jth measurement time tag, ρ_{SVi} is the corresponding pseudorange measurement from the ith GPS satellite vehicle, $\mathbf{r}_{SVi}$ is the position of *SVi* based on its broadcast ephemeris, and δt_T is a correction to the time tag, also based on broadcast parameters, accounting for the time at which the measurement signal was transmitted. The notation $\|\ \|$ denotes the Euclidean norm. The remaining terms in (2) describe corruptions to the measurement: c is the chaser receiver clock bias, also accommodating any biases common to all receiver channels, and b_{SVi} is a range bias parameter unique to each *SVi*, tuned to accommodate SA and other unmodeled radio frequency propagation biases unique to a given receiver channel. I_{SVi} is a correction for single-frequency ionospheric refraction based on a model due to Lear (ref. 8, pp. 6-1 to 6-7 and A-1 to A-10), and v_j is a noise sequence. In specifying the statistics of v_j, δ_{jk} denotes the Kronecker delta function, and the variable σ_v^2 is the noise variance. We assume that the measurement noises from each of the *SVi* are uncorrelated. To model the clock bias, we assume that it is the integral of a drift variable, d. The drift, d, is modeled as a first-order Gauss-Markov process. First-order Gauss-Markov processes are also the models we choose for each of the four range bias variables, which we assume are uncorrelated and equally distributed.

SVM for the filter is based on (1) and (2). In this mode, the filter state vector is based on the unknown variables in these two equations. Therefore, the filter must estimate these variables. The 15-element state vector for this mode, $\mathbf{x}_{sng}$, is defined as

$$\mathbf{x}_{\mathrm{sng}} = \left[\mathbf{r}_c^{\mathrm{T}}, \mathbf{v}_c^{\mathrm{T}}, c, d, \delta\mathbf{a}_u^{\mathrm{T}}, \mathbf{b}_c^{\mathrm{T}}\right]^{\mathrm{T}}$$

where the range biases for the four channels of the chaser receiver have been collected in the vector $\mathbf{b}_c$. This vector is initialized, propagated, and updated in an extended Kalman filter recursion (ref. 7, pp. 182-188). Whenever satellite switching occurs on a given receiver channel, the filter state corresponding to that channel's range bias is reinitialized. Next we will describe relevant details of our implementation of the models described above in the Kalman filter.

The state vector is analytically propagated between measurements, except for the chaser position and velocity elements, integrated numerically using the "Super-G" integrator (ref. 9, p. 4-130). The Kalman filter recursion also requires that we propagate the covariance matrix corresponding to state vector estimation errors,

$$\bar{\mathbf{P}}(t_j) = \Phi(t_j, t_{j-1})\hat{\mathbf{P}}(t_{j-1})\Phi^{\mathrm{T}}(t_j, t_{j-1}) + \mathbf{S}(\Delta t) \tag{3}$$

where $\bar{\mathbf{P}}(t_j)$ is the covariance just prior to incorporating the measurements at t_j into the state and $\hat{\mathbf{P}}(t_{j-1})$ is the covariance just after incorporating the measurements at t_{j-1}. The matrix functions $\Phi(t_j, t_{j-1})$ and $S(\Delta t)$ are based on (1), but we make several assumptions and approximations in deriving them. The matrix Φ, corresponding to the state error transition, is nominally the solution of the matrix differential equation $\dot{\Phi}(t_j, t_{j-1}) = \mathbf{F}(t_j)\Phi(t_j, t_{j-1}), \Phi(t_{j-1}, t_{j-1}) = \mathbf{I}$ where $\mathbf{F}(t_j)$ is the Jacobian matrix of the state vector, evaluated at the latest estimate. However, we approximate the upper six-by-six partition of $\mathbf{F}$ by assuming a spherical Earth. Assuming $\mathbf{F}$ is constant over the propagation interval, the solution for Φ is given by the matrix exponential $e^{\mathbf{F}\Delta t}$. For the upper six-by-six partition, we approximate the exponential with a second-order truncation of its representation as an infinite series (ref. 10, p. 55). The remaining diagonal elements of Φ correspond to state transitions of first-order Gauss-Markov processes except in the case of the clock bias, which is the integral of the drift. Since for any first-order Gauss-Markov process the state transition is $e^{-\Delta t/\tau}$, we can easily show the state transition for the clock bias and the rift elements of Φ has the form

$$\Phi_{\mathrm{clock}}(\Delta t) = \begin{bmatrix} 1 & \tau(1 - e^{-\Delta t/\tau}) \\ 0 & e^{-\Delta t/\tau} \end{bmatrix}$$

Clearly, most of the elements of Φ are zeros. We exploit this structure by using sparse matrix operations in coding (3).

Most of the discrete process noise matrix S in (3) results from an analytic solution of the well-known integral (e.g., ref. 7, p. 77) $\int_0^{\Delta t} \Phi(t, s)\mathbf{G}\mathbf{Q}\mathbf{G}^{\mathrm{T}}\Phi^{\mathrm{T}}(t, s)ds$, where the matrix Q is the spectral density of the 11-element process noise vector (3 for direct process noise, 1 for clock drift, 3 for unmodeled acceleration, and 4 for the range biases), and G is a matrix of ones and zeros mapping these 11 terms into the 15-element state vector. The exception is the upper six-by-six partition involving the state transition of the position and velocity and the direct process noise spectral density. Following an approach similar to Lear's (ref. 11, p. 172), we dispense with the continuous time model shown in (1) and instead assume the direct process noise is a discrete sequence of step functions, constant over the filter propagation interval. The result has the following simple form:

$$\mathbf{S}_{wd} = \sigma_{wd}^2 \begin{bmatrix} \Delta t^4/4\,\mathbf{I}_3 & \Delta t^3/3\,\mathbf{I}_3 \\ \Delta t^3/3\,\mathbf{I}_3 & \Delta t^2\mathbf{I}_3 \end{bmatrix}$$

where $\mathbf{I}_3$ is the three-by-three identity matrix. As with the state transition matrix, we exploit sparsity in the process noise matrix in coding (3).

In addition to using the covariance for the standard Kalman gain calculations, we use it for measurement screening. Prior to incorporating a measurement, the filter differences it with its predicted value, based on the latest state estimate. This difference is often called the filter innovation, and its variance is computed as part of the standard filter recursion. We divide the filter innovation by its variance and reject any measurements exceeding a given dimensionless threshold. For our filter, we chose 10 as the threshold.

Dual-Vehicle Mode

When RPO receives target GPS measurements, the filter automatically reinitializes and transitions to DVM. At this point, the filter augments its state vector and covariance with target position and velocity elements, target receiver clock bias and drift, and 8 additional range biases for the 8 channels in the TurboRogue receiver, bringing the total number of states to 31. The filter state time is referenced to the chaser state time for both vehicle states. The model described in (1) for chaser position and velocity propagation is used for the target vehicle as well, except we do not employ unmodeled acceleration for the target, and different tuning parameters may be specified. The target receiver clock model, as well as the additional range biases for the target receiver, employ the same models as the chaser range biases, but the clock model may have different tuning parameters. An explicit relative state is not estimated by the filter. Rather, it generates an estimate of the chaser and target inertial states, and RPOP computes the relative side.

A key filter performance discriminator and element of the filter design is exploitation of satellite commonality between the target and the chaser. Whenever the two receivers are tracking a common GPS satellite, the same range bias element of the state vector is used for both. This is the only direct coupling between target and chaser states in the filter. As shown by Montez and Zyla (ref. 2), when two vehicles are in moderately close proximity, simultaneously estimating a common range bias from pseudorange measurements is an effective strategy for nullifying the effects of SA. When four common satellites are tracked by both receivers, only those common channels are processed. Whenever there are less than four common satellites the filter processes all available measurements from the receivers on both vehicles. During the periods of uncommon satellite tracking, the range bias estimation performance is important to minimize the effect of SA on the relative state accuracy.

The relative state performance is also sensitive to the minimum number of satellites available for processing from each GPS receiver. Pseudoranges from an least four satellites must be processed for both chaser and target filter paths to ensure the expected orbit estimation accuracy. Additionally, the receiver clock bias and drift rate estimation hinges on the stability of the clocks. The clock drift rates are modeled essentially as random constants, exponentially correlated random processes with the time constant value of 200,000 sec. Based on preflight experience with Osborne/JPL TurboRogue GPS data collected from another orbital mission and during an integrated test performed at the Kennedy Space Center, the time constant value of the receiver clock drift rate of the target filter was lowered to 2000 sec. This was necessary to accommodate the occasional oscillatory behavior of the clock bias estimates from the TurboRogue receiver. Other performance discriminators include the likeness of modeling filter state noise, ionospheric correction, and the inertial measurement unit (IMU) data processing effect between two filter paths.

Once the transition to DVM has occurred, the filter cannot switch back to SVM unless it is manually reinitialized. If all target measurements drop out, the filter will continue to process any available chaser measurements. During these data dropouts, the filter propagates the state and covariance for the target position and velocity and the additional range biases. This strategy avoids filter reinitialization and the resulting inaccurate transient solutions during periods of intermittent communications between the vehicles.

Results

The flight experiment produced a significant amount of GPS data from the receivers of both the Orbiter and the WSF, including over 5 days of 3M GPS data and about 19 hours of TurboRogue receiver data. Postflight replay and the RGPS filter performance studies will use these data. In addition, the ground test facilities for ATV and ISS will also use these data for model validation and design analysis. Below, we will first present results from real-time onboard data processing and from near-real-time analysis performed in the Mission Control Center (MCC). Then we will present the results obtained by running the filter in a real-time mode using recorded data.

Real-Time Onboard Processing

This section will show and explain results from data generated in real time onboard by the RGPS filter during the mission. The SVM results will be followed by the DVM results.

Single-Vehicle Mode. During most of the data collection periods for the Orbiter 3M GPS receiver, the 15-state SVM of the RGPS filter performed real-time orbit determination in SVM. To our knowledge, the 15-state Kalman filter is the largest state-size filter ever used for real-time GPS orbit determination onboard a spacecraft. As the semimajor axis (SMA) comparison, Figure 7 demonstrates that the RGPS output shows much smoother estimates than those of the 11-state 3M receiver filter output. The smoother SMA estimates can be attributed to the range bias states used in the RGPS filter to model the effects of SA. Figure 7 also includes the FOM, a normalized standard deviation of the predicted SMA error with respect to the steady-state expected value (75 m in this experiment). Therefore, the FOM is an indication of filter convergence.

Several problems related to the 3M receiver contributed to the inferior SMA solutions from both the RGPS filter and the receiver. Some of the erratic behavior in the 3M solution data can be attributed to a known software limitation in the 3M receiver when operating in C/A mode. The 3M receiver was specifically designed as a dual-frequency, P-code receiver. This limitation results in very large SMA transients (outside the scale of Figure 7). The RGPS SMA solutions were noisier than expected because of the inadvertent processing of measurements from the fifth 3M receiver hardware channel. The Collins 3M receiver has five hardware channels, but the fifth channel roves among all visible satellites. Since the dwell time on each channel is short, we intended not to exploit this hardware channel in the RGPS filter. The information received by the filter contained the first four "software" channels. Unfortunately, these software channels randomly switch among all five hardware channels, resulting in the filter inadvertently processing these rapidly changing satellites. Each time a new satellite is processed, the range bias state is reinitialized, preventing range bias convergence.

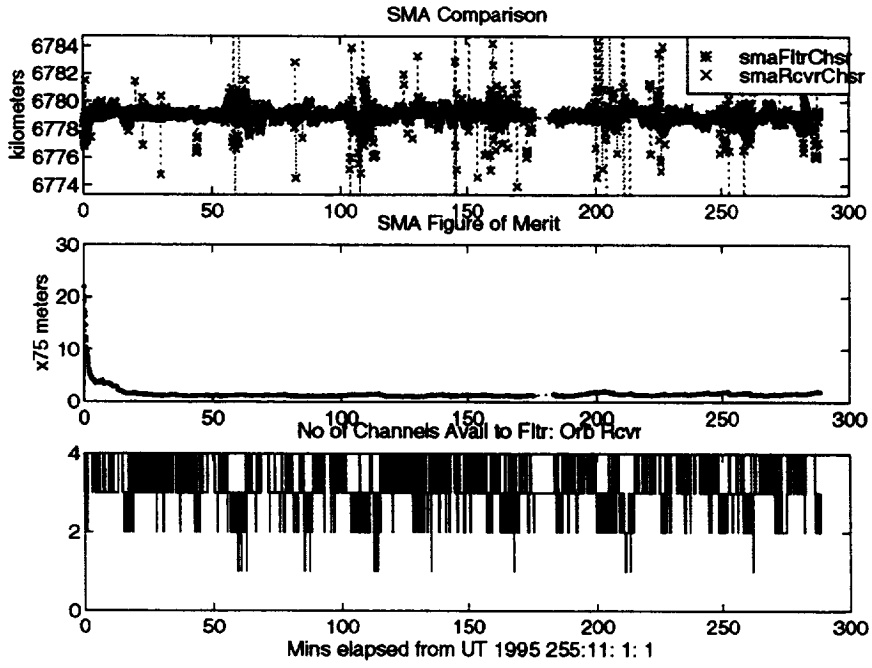

Figure 7: Real-time onboard SVM results

Dual-Vehicle Mode. A few snapshots of WSF GPS data became available during the WSF free-flight. However, hands-off operation of the RGPS filter did not transition from SVM to successful DVM operation, owing to an unexpected set of stale data that preceded fresh WSF GPS data at the beginning of each snapshot. The filter target state was repeatedly initialized using several hours-old solutions, causing all target GPS measurements to be rejected. Successful DVM operation could have been achieved with a manual reinitialization of the filter. Note, the snapshots were intended to allow a quick assessment of WSF GPS receiver performance. DVM operation in this period was not intended to demonstrate filter performances since the data availability interval was planned to be too short for filter convergence. Ground examination of downlinked GPS data uncovered this stale leftover data problem. The filter successfully processed the snapshot data in DVM during near-real-time RPOP/RGPS execution of these downlinked data in the MCC. This was achieved by delaying the reinitialization of the filter until fresh data arrived.

Figure 8a shows the SMA solutions from the receivers and the RGPS filter during this short snapshot period. Figure 8b shows the SMA FOM in the transient phase for the target and the chaser, and the corresponding relative SMA filtered error standard deviation. Figure 8c shows the number of channels tracked by each receiver during the snapshot. As Figure 8c shows, the number of satellites being tracked by each receiver was low, resulting in very poor common satellite tracking during this period. The brevity of the WSF GPS snapshot availability did not allow the filter enough time to converge. The combination of these two effects resulted in rather high SMA FOM values during this period. Note that the SMA estimate convergence takes 20 to 30 minutes of filter operation under the minimum of four-satellite coverage.

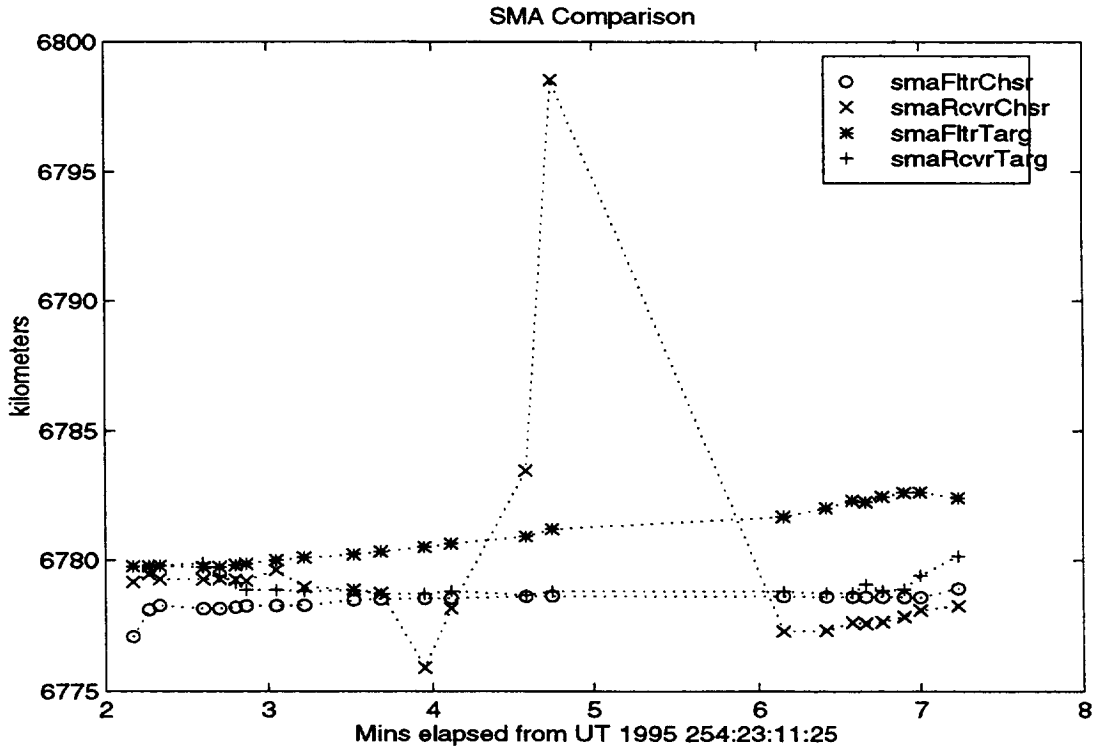

Figure 8a: SMA comparison during near-real-time processing of snapshot data

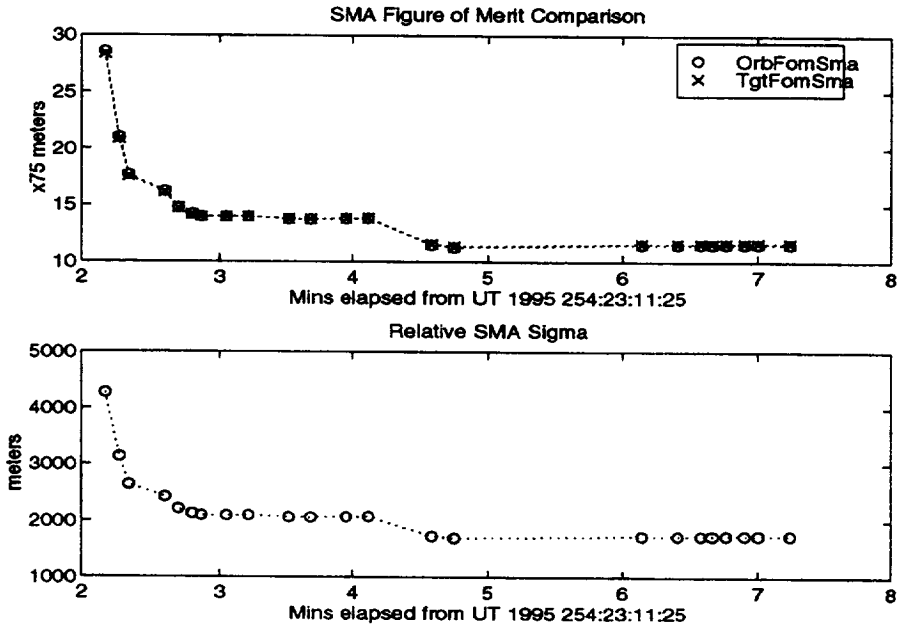

Figure 8b: SMA parameters during near-real-time processing of snapshot data

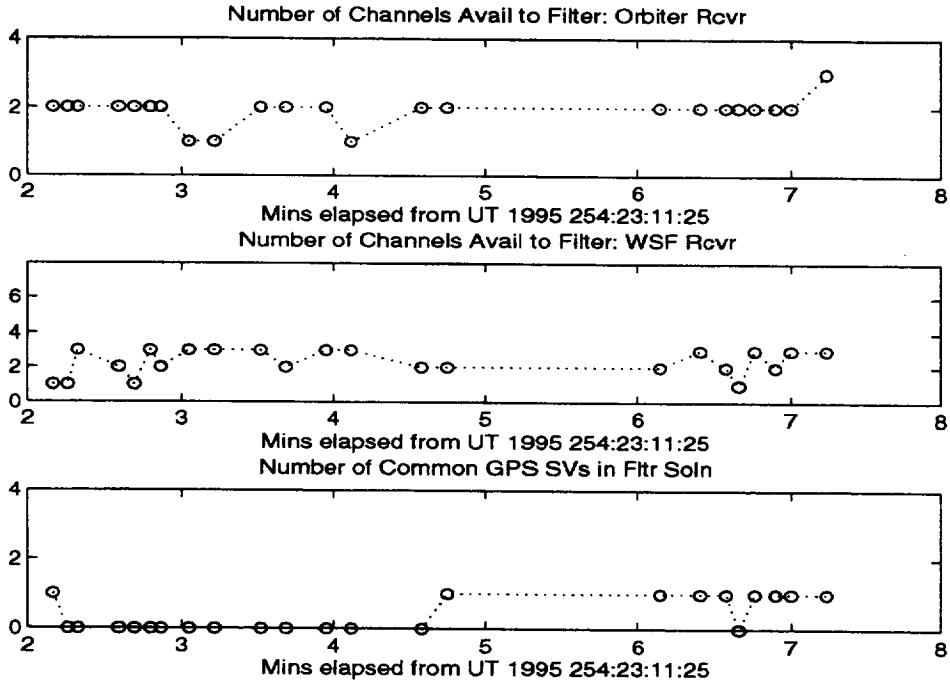

Figure 8c: Number of channels tracked by each receiver snapshot

Postflight Processing of Recorded Data

As previously explained, continuous WSF GPS data never became available during WSF rendezvous. To complete the performance analysis, we ran RPOP/RGPS in a real-time mode using recorded data. Results from these RPOP/RGPS runs were compared to the BET generated by UT/CSR described by Schroeder et al. (ref. 3). At the time of this publication, the BET was only available for approximately 4 hours of the time just following WSF deploy. However, we limited our comparisons to approximately 1 hour because of the unexpected clock bias behavior of the TurboRogue receiver. Below we will explain the TurboRogue clock bias behavior, and then compare SVM and DVM results to the BET.

TurboRogue Receiver Clock Offset Problem. The postflight analysis revealed unexpectedly inferior behavior in the TurboRogue clock offset. Figure 9 shows an almost periodic random behavior of substantial magnitude. This behavior may be due to a feedback loop present in the receiver clock-steering algorithm. The second-order Markov clock model and the associated tuning parameters used in the RGPS filter assume a slowly drifting clock behavior common to the majority of GPS receiver clocks. We, therefore, limited our comparisons to a segment of relatively mild clock behavior.

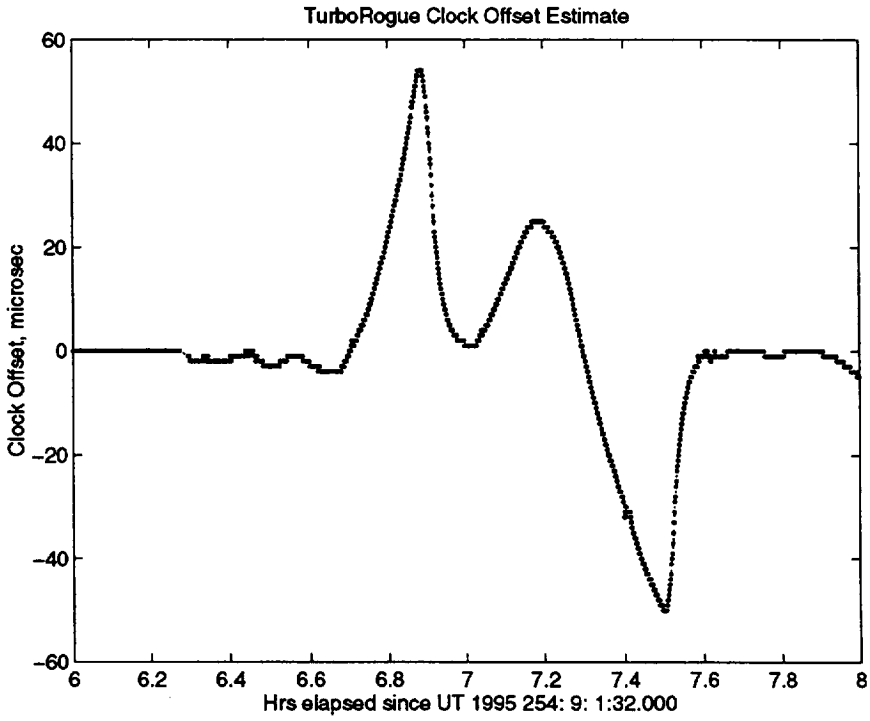

Figure 9: TurboRogue receiver clock offset

Single-Vehicle Mode. Figure 10 presents the results of SVM operations compared to the BET. The plots in the left column of Figure 10 reveal the position differences in UVW (radial, downtrack, and cross-track) coordinates as well as the SMA differences between the SVM solutions and the BET. In the right column, the 3M receiver and the Space Shuttle RNAV solutions are compared to the BET. Note that the state estimates from RGPS filters are superior.

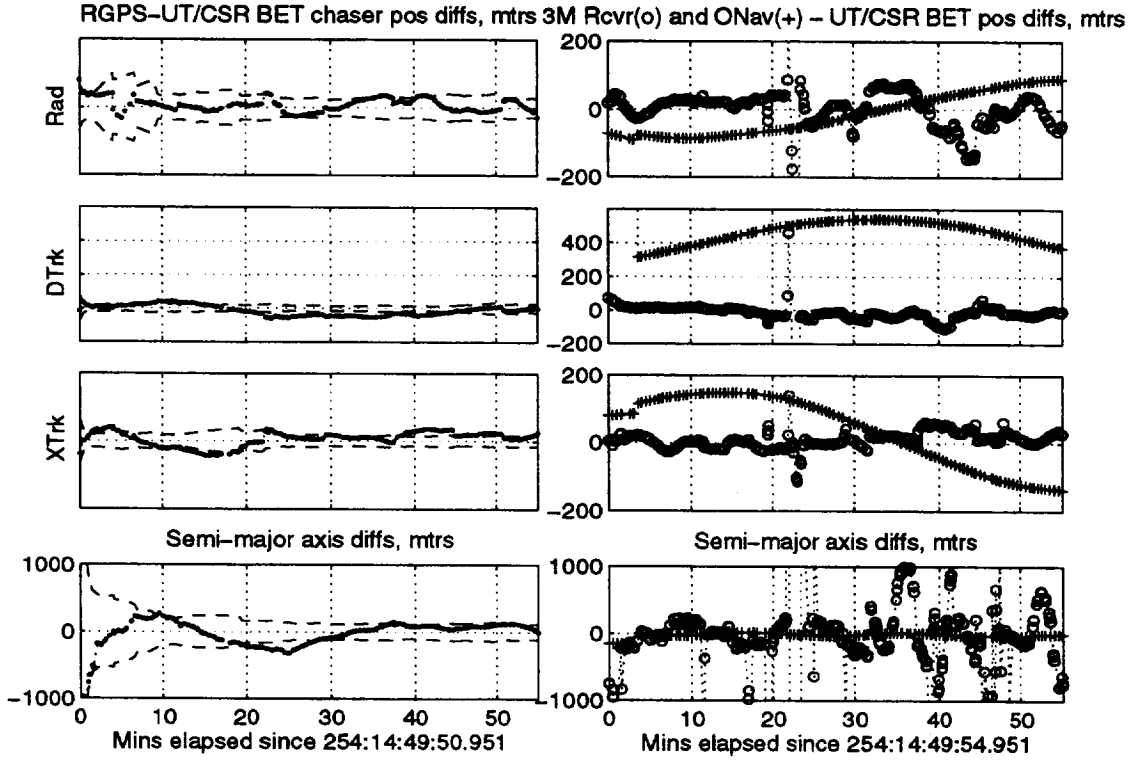

Figure 10: SVM position and SMA differences from postflight processing

Figure 11 shows a comparison of SMA solutions from several sources. Note that the first two and the last three RGPS filter marks were sampled from the real-time STS-69 onboard results, while the three marks in the middle were obtained from the post-mission replay. The marks labeled MCC are near-real-time, batch-to-batch solutions generated from the MCC using tracking and data relay satellite system (TDRSS) measurements as an independent performance check. Comparisons between the RGPS filter, the BET, and the MCC TDRSS solutions uncovered an unexpected redundant compensation of the 3M receiver clock bias on its data during initialization of the RGPS filter. We confirmed that the 3M receiver output its solution and raw measurements with compensated time tags based on its clock bias solution. Since this was not realized before the mission, the RGPS filter was also compensating for the clock bias resulting in redundant compensation of the clock bias on the 3M receiver output. This redundant compensation results in somewhat degraded RGPS solutions.

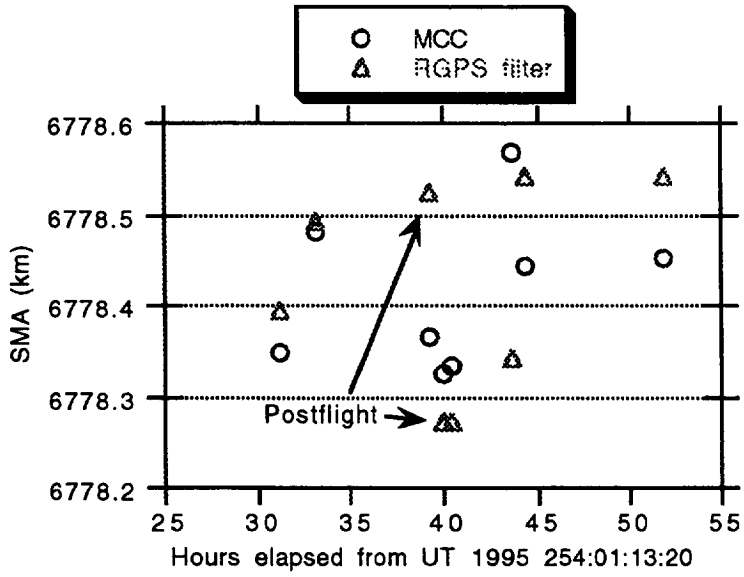

Figure 11: Comparison of SMA estimates

Dual-Vehicle Mode Playback. Figure 12 shows the relative trajectory from the BET, RGPS filter, and GPS receiver deterministic solutions in target-centered local vertical/local horizontal (LVLH) coordinates. The RGPS filter compares more favorably to the BET than does the receiver deterministic solution, as expected. Figure 13 demonstrates the position state differences between the RGPS filter output and the BET in UVW coordinates, as well as the SMA difference profile. Both the absolute state differences of the chaser state as well as the relative state differences show close agreements, and the filter-predicted error standard deviation closely follows the estimation error behavior.

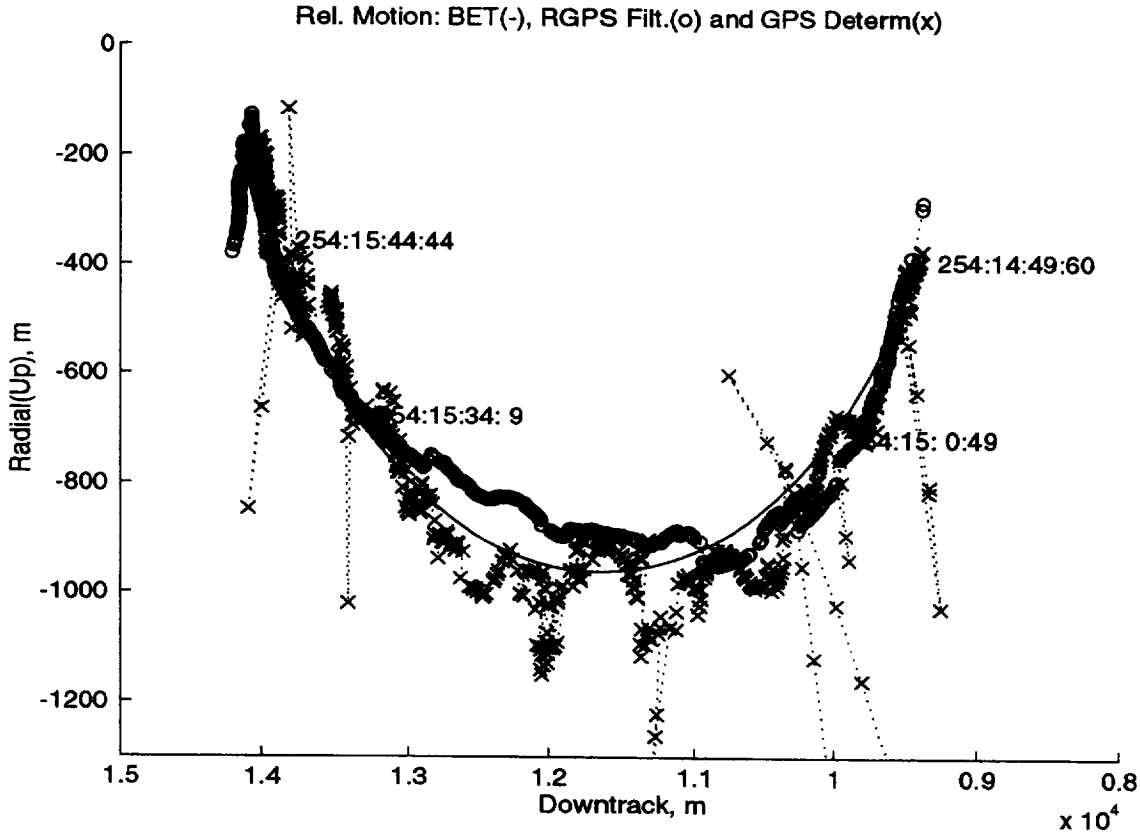

Figure 12: Target-centered relative motion plot

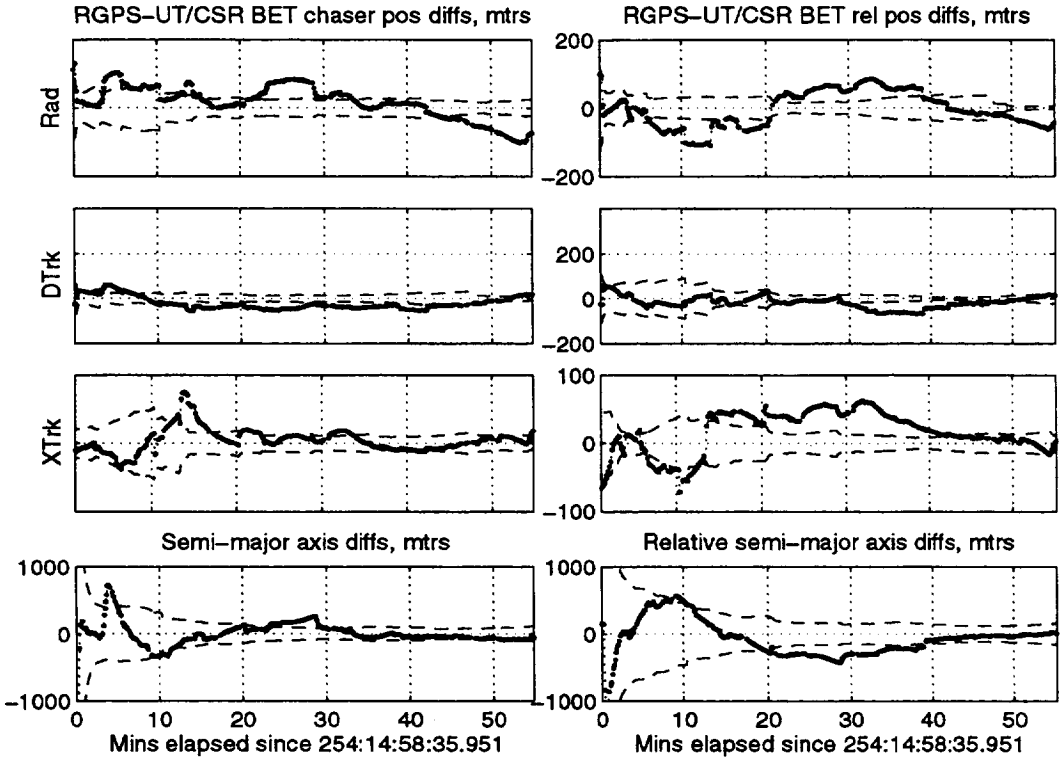

Figure 13: DVM position and SMA difference from postflight processing

As indicated by Figure 14, the satellite coverage over the period of the run is not adequate. Specifically, the number of common satellites did not achieve the required value of four, essential for achieving the potential level relative GPS accuracy.

Overall the RGPS filter performance in DVM was quite satisfactory, given the unexpected clock offset problems, the poor satellite coverage, and the reduced number of common satellites available. The clock problem presented the most severe performance limitation, besides the lack of common satellites, in achieving expected relative state accuracy. Note that the effect of SA on the chaser and the target absolute state estimates causes a degraded relative state estimate when the common satellite bias cancellation is not present.

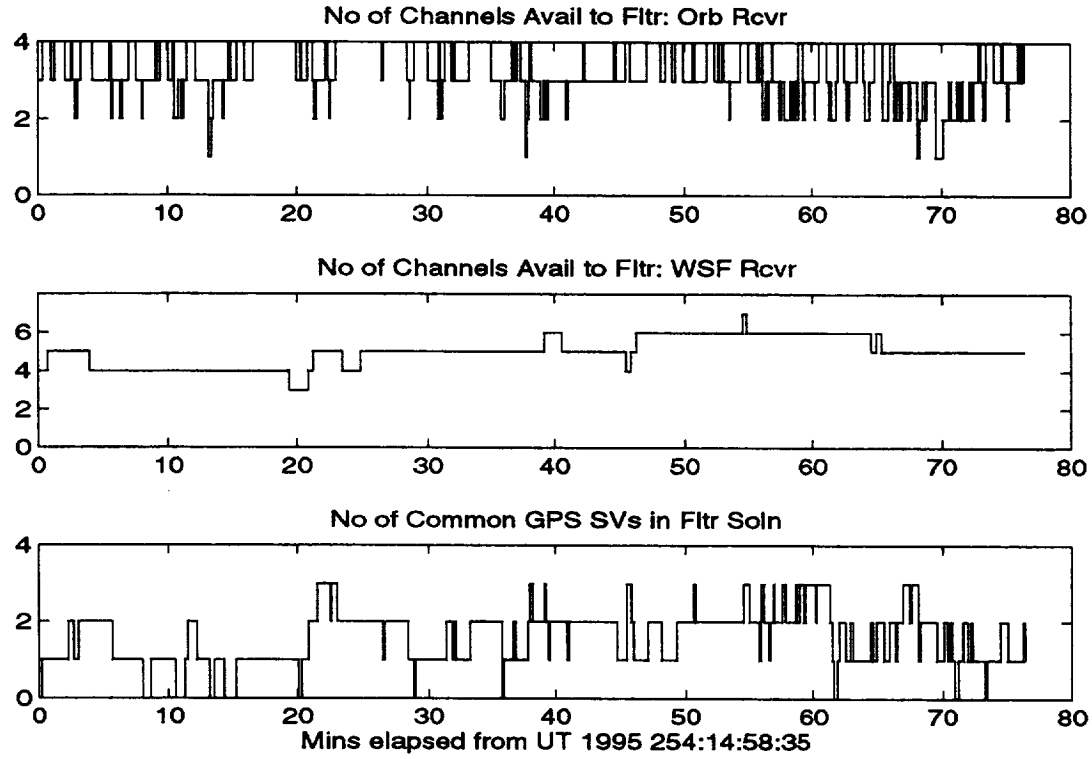

Figure 14: Common satellite availability from postflight processing

Conclusions

The real-time DVM operation was disappointingly short owing to the limited availability of data from two GPS receivers during WSF free-flight. Nonetheless, an extensive exercise of the 15-state orbit determination filter in SVM has yielded an unprecedented real-time GPS data filtering experience and database. This represents the largest known state-size orbit-determination filter ever flown on a spacecraft to process GPS measurements and to solve for the effects of SA. In addition, postflight analysis was performed running the RGPS filter in a real-time mode using data recorded onboard the Orbiter and the WSF during the mission. This analysis has demonstrated the performance of relative state estimation under conditions of dissimilar receivers, SA, and non-common satellite visibility. The following is a list of valuable lessons learned:

1. Satellite commonality, crucial in achieving accurate relative state estimates, is not easily achieved.

2. The effect of SA can be significantly reduced by modeling range bias states, as demonstrated in the comparison of the filtered to the receiver-computed relative states and SMA estimates. Therefore, it is a viable and worthwhile strategy for single-vehicle orbit determination as well as the relative state navigation in spacecraft GPS applications.

3. When there is only one state time tag for both vehicle states, clock bias estimation errors in one receiver will affect the filter's processing of both receiver's data.

4. Real-time data can behave unpredictably. Emphasis must be placed on efforts to protect against as many data failure situations as possible.

5. For the class of GPS receivers with a clock steering algorithm, the clock parameter modeling presents a significant challenge. To overcome this problem for orbital applications, disabling the clock steering algorithm may be required.

Despite many hardware and software glitches encountered during the mission, valuable lessons have been learned. The next opportunity to fly this experiment will be later this year (1996) on STS-80.

Acknowledgments

The project, the results of which are reported here, was supported and funded by the ISS Phase One Risk Mitigation Office. Also, without the contributions of the following people our results could never have been achieved: P. A. M. Abusali, Antha Adkins, Nick Combs, Gene Cook, Mike Cooke, Scott Cryan, Brent Disselkoen, Charley Dunn, Courtney Duncan, Mike Exner, Ron Flanary, Bill Jackson, Jim Ledet, Kevin Lee, Stephanie Lowery, Rick McCloskey, Samantha McDonald, Charlene Madden, Tom Manning, Scott Merkle, Tim Minnix, Moises Montez, Dave Mulcihy, Tri Nguyen, Ray Nuss, John Riehl, Penny Saunders-Roberts, Christie Schroeder, Bob Schutz, Tom Silva, Charles Simmons, Scott Tamblyn, and Dave Walker.

References

1. Hinkel, H. D., Y.-W. Park, and W. Fehse, "Realtime GPS Relative Navigation Flight Experiment," *Proceedings of the National Technical Meeting*, The Institute of Navigation, January 1995, pp. 593-601.
2. Montez, M., and L. Zyla, "Use of Two GPS Receivers in Order to Perform Space Vehicle Orbital Rendezvous," *Proceedings of the ION GPS-93*, The Institute of Navigation, September 1993, pp. 301-312.
3. Schroeder, C., B. Schutz, and P. Abusali, "STS-69 Relative Positioning GPS Experiment," *AAS/AIAA Conference*, Paper No. AAS 96-180, February 1996.
4. Saunders, P. E., et al., "The First Flight Tests of GPS on the Space Shuttle," *Proceedings of the 1994 ION National Technical Meeting*, The Institute of Navigation, January 24-26, 1994.
5. Schutz, B., et al., "GPS Tracking Experiment of a Free-Flyer Deployed from Space Shuttle," *Proceedings of the ION GPS-95*, The Institute of Navigation, September 1995, pp. 229-235.
6. March, J. G., et al., "Gravity Model Improvements Using Geos 3 (GEM 9 and GEM 10)," *Journal of Geophysical Research*, Vol. 84, No. B8, July 30, 1979.
7. Gelb, Arthur (ed.), *Applied Optimal Estimation*, The M.I.T. Press, Cambridge, Mass., 1974.
8. Lear, W. M., "Proposed Simplified GPS Navigation Filters," JSC-25468 (Rev. 1), NASA Johnson Space Center, Houston, Texas, 1993.
9. "Space Shuttle Operational Level C Functional Subsystem Software Requirements: Guidance, Navigation, and Control: Part B: Onorbit Navigation," STS 83-0006H (OI-24), Rockwell International Space Systems Division, 1993.
10. Chen, C.-T., *Linear System Theory and Design*, Holt, Rinehart, & Winston, Inc., New York, 1984.
11. Lear, W. M., "Kalman Filtering Techniques," JSC-20688, NASA Johnson Space Center, Houston, Texas, 1985.

REPORT DOCUMENTATION PAGE

Form Approved
OMB No. 0704-0188

1. AGENCY USE ONLY (Leave Blank)	2. REPORT DATE	3. REPORT TYPE AND DATES COVERED
	November 1996	NASA Technical Memorandum

4. TITLE AND SUBTITLE

Flight Test Results from Real-Time Relative Global Positioning System Flight Experiment on STS-69

5. FUNDING NUMBERS

6. AUTHOR(S)

Young W. Park*; Jack P. Brazzel*; J. Russell Carpenter; Heather D. Hinkel; James H. Newman

7. PERFORMING ORGANIZATION NAME(S) AND ADDRESS(ES)

Lyndon B. Johnson Space Center
Aeroscience and Flight Mechanics Division
Houston, Texas 77058

8. PERFORMING ORGANIZATION REPORT NUMBERS

S-821

9. SPONSORING/MONITORING AGENCY NAME(S) AND ADDRESS(ES)

National Aeronautics and Space Administration
Washington, D. C. 20546-0001

10. SPONSORING/MONITORING AGENCY REPORT NUMBER

TM-104824

11. SUPPLEMENTARY NOTES

*McDonnell Douglas Aerospace, Houston, Texas

12a. DISTRIBUTION/AVAILABILITY STATEMENT

Unclassified/Unlimited
Available from the NASA Center for AeroSpace Information (CASI)
800 Elkridge Landing Road
Linthicum Heights, MD 21090-2934
(301) 621-0390 Subject Category: 17

12b. DISTRIBUTION CODE

13. ABSTRACT *(Maximum 200 words)*

A real-time global positioning system (GPS) Kalman filter has been developed to support automated rendezvous with the International Space Station (ISS). The filter is integrated with existing Shuttle rendezvous software running on a 486 laptop computer under Windows*. In this work we present real-time and postflight results achieved with the filter on STS-69. The experiment used GPS data from an Osborne/Jet Propulsion Laboratory TurboRogue receiver carried on the Wake Shield Facility (WSF) free-flyer and a Rockwell Collins 3M receiver carried on the Orbiter. Real-time filter results, processed onboard the Shuttle and replayed in near-real time on the ground, are based on single-vehicle mode operation and on 5 to 20 minute snapshots of telemetry provided by WSF for dual-vehicle mode operation. Postflight results were achieved by running the filter in real-time mode using data recorded during the mission. Orbiter and WSF state vectors calculated using our filter compare favorably with precise reference orbits determined by the University of Texas Center for Space Research. The lessons learned from this experiment will be used in conjunction with future experiments to mitigate the technology risk posed by automated rendezvous and docking to the ISS.

*Trademark

14. SUBJECT TERMS	15. NUMBER OF PAGES
global positioning system; space rendezvous; real time operation; Kalman filters	25
	16. PRICE CODE

17. SECURITY CLASSIFICATION OF REPORT	18. SECURITY CLASSIFICATION OF THIS PAGE	19. SECURITY CLASSIFICATION OF ABSTRACT	20. LIMITATION OF ABSTRACT
Unclassified	Unclassified	Unclassified	Unlimited